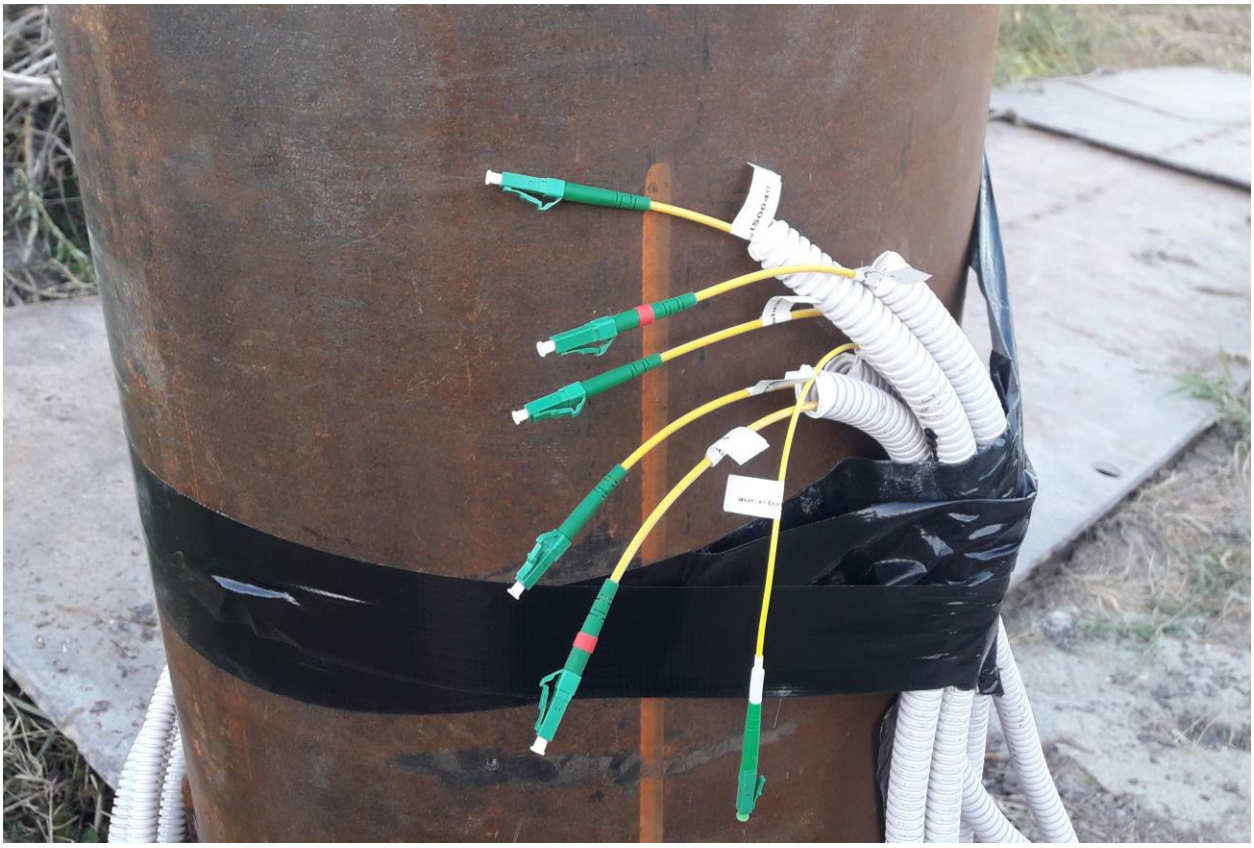

Kania, J.G, Sorensen, K.K., and Fellenius, B.H., 2024. The development of unit shaft resistance along driven piles in subsiding soil. Canadian Geotechnical Journal, 59(6) 1-16.

Canadian Geotechnical Journal

Article

The development of unit shaft resistance along driven piles in subsiding soil

Jakub G. Kania[a], **Kenny K. Sørensen**[b], **and Bengt H. Fellenius**[c]

[a]Department of Engineering, Aarhus University, Aarhus, Denmark; [b]Department of Civil and Architectural Engineering, Aarhus University, Aarhus, Denmark; [c]British Columbia, Sidney, Canada

Corresponding author: **Kenny K. Sørensen** (email: kks@cae.au.dk)

Abstract

The influence of bitumen coating on the development of unit shaft resistance along driven steel and precast concrete piles resulting from subsiding surrounding soft soil (gyttja) induced by fill placement at terrain was investigated. All piles were instrumented with conventional discrete-point vibrating wire strain gauges and distributed fibre optic sensors to achieve high-resolution strain measurements. The magnitude of the mobilised unit shaft resistance along uncoated piles was observed to be primarily related to an increase in effective stress resulting from the dissipation of excess pore water pressures. The unit shaft resistance along bitumen-coated piles was found to be primarily related to the rate of relative movement between pile and soil, which highlights the effectiveness of bitumen coating in reducing shaft resistance.

Key words: soil–pile interaction, bitumen coating, instrumented piles, fibre optic sensors, drag force, negative skin friction

1. Introduction

In a subsiding soil, the sum of the sustained load on the pile plus the drag force (due to accumulated negative skin friction) above the "neutral plane" (N.P.) is in equilibrium with the sum of the positive shaft resistance and the mobilised toe resistance below the N.P. Because the transition at the N.P. from negative to positive direction of shaft resistance involves a gradual movement change, a transition zone will develop above and below the N.P.

The first full-scale pile tests investigating negative skin friction employed telltales to obtain the force distribution (Johannessen and Bjerrum 1965; Bjerrum et al. 1969; Endo et al. 1969). However, one limitation with telltales is that measurements are only obtained after driving. This disadvantage can be eliminated by using load cells, strain gauges, or vibrating wire (VW) strain gauges directly attached or embedded in a test pile. Fellenius and Broms (1969) and Fellenius (2006) reported load-cell results concerning force distribution and effects of pile installation, soil reconsolidation, pile head loading, and placing fill around the test piles. Such sensors can, however, only provide strain data at discrete points. To overcome the limitations of discrete-point measurements, recent studies (e.g., Klar et al. 2006; Kania et al. 2020) have shown the advantage of using distributed fibre optic sensors (DFOS) to obtain high-resolution measurements of the axial force distribution in both driven and bored piles.

Previous full-scale tests have been mainly performed to study the development of drag force and downdrag along steel and precast concrete driven piles installed in soft marine clay (Johannessen and Bjerrum 1965; Bjerrum et al. 1969; Endo et al. 1969; Okabe 1977; Indraratna et al. 1992; Fellenius 2006). Little information is available on the subject for driven piles installed in gyttja, a typical organic soft soil of Denmark, which has not been widely studied. In regard to piled foundation design, the current edition of the Euro Code adds drag force to the load from the supported structure or disregards contribution to bearing from layers with negative skin friction. Therefore, it was considered important to investigate the magnitude and mechanism of drag-force build-up for piles installed in similar ground conditions as the subject site.

To reduce the drag force, Baligh et al. (1978) proposed electroosmosis, placing a casing outside the pile, or coating the pile with bitumen, of which the bitumen coating is considered the most efficient method. The efficiency of bitumen coating is controlled by the shearing rate, thickness of the bitumen coating, and temperature (Hutchinson and Jensen 1968; Fellenius 1979). The typical coating used in the previous studies was Penetration Graded Bitumen 60/70 or 80/100 (ASTM D946M) with a thickness of about 1–1.5 mm.

In July 2018, an experimental programme was started in Randers, Denmark, to investigate force distribution in four uncoated and bitumen-coated, steel and precast concrete, instrumented piles driven in compressible gyttja. The experimental programme was carried out as part of a larger research study into soil–structure interaction in soft soils (Kania 2020). The piles were instrumented with DFOS and VW strain gauges. The details of the used Rayleigh-based DFOS system and general application of DFOS in piles were presented by Kania et al. (2020). Subsidence was induced by placing a 2 m thick fill around the test piles.

Fig. 1. Soil properties: (A) Atterberg limits and water content and (B) undrained shear strength. LL, liquid limit; PL, plastic limit.

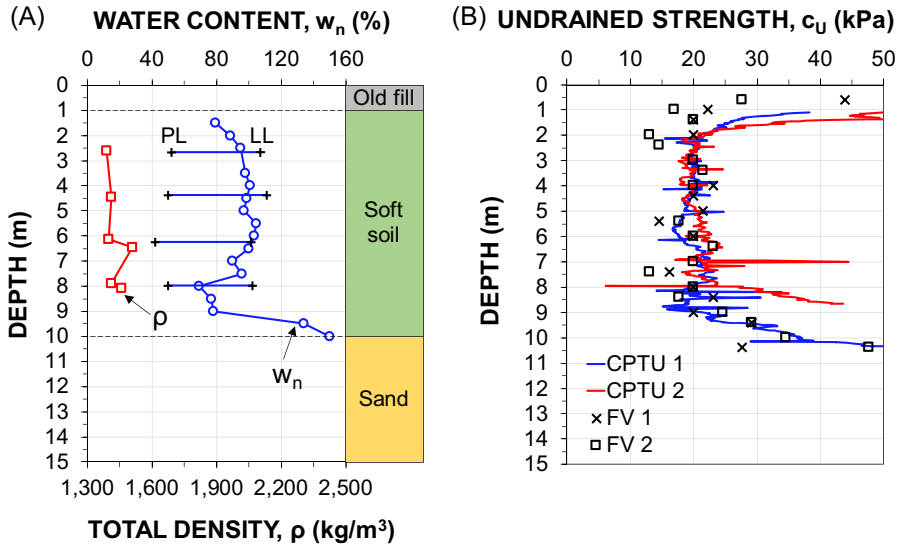

DFOS were utilised in the project to provide significantly greater depth resolution in the strain measurements and hence force distribution within the instrumented piles than seen in previous reported studies on driven piles in subsiding soft soils.

2. Materials and methods

2.1. Soil and ground water conditions

The test site was located at Randers Harbour, Denmark (ETRS89 UTM32N 565559, 6257861). The soil profile consisted of 1 m old fill above an 8–10 m thick soft soil layer overlying a postglacial, marine, medium dense sand. The ground surface was at an elevation of ±0.0 m (per Danish Vertical Reference 1990) prior to fill placement, and the water pressure in the sand layer is slightly artesian rising to a mean level of ele-vation +0.7 m. The perched water table in the old fill was observed in a shallow trench to be about 0.4 m below the ground surface.

The soft soil layer is gyttja, a postglacial organic clayey sandy silt of marine origin containing sporadic shell fragments (up to approximately 20 mm in size). Gyttja originates from decomposed remains of plants and microscopic animals mixed with mineral particles.

The grain size distribution was determined by laser diffraction performed on four soil samples from different depths (Savery 2019) and showed, on average, that the dominant particle size was silt (75%–81%), the clay size fraction was 16%, and the sand size fraction was 7%. The organic content ranged from 7.5% to 9.1% with an average of about 8%.

Figure 1 shows (A) the distribution of water content and soil density and (B) the undrained shear strength determined from field vane test (FV) and cone penetration tests (CPTU). The depth refers to the depth below the original ground surface.

The water content, w_n, of the soft soil layer was found to range from about 70% to about 150% and was generally close to the liquid limit, LL, which was found to range from about 101% to 111%. The lower about 1 m thick layer of the soft soil had larger water content and was of more peaty nature. The plastic limit, PL, and plasticity index, IP, ranged from 42% to 52% and from 50% to 62%, respectively. The unit densities, ρ, of the soft soil layer ranged from 1390 to 1510 kg/m^3 with an average value of 1430 kg/m^3.

The undrained shear strength (field vane test), $c_{u,FV}$, of the soft soil was adjusted by a factor $k = 0.77$ based on the plasticity index, IP (Bjerrum 1972), and ranged from 13 to 35 kPa with an average of 21 kPa. The sensitivity of the soft soil, S, (the ratio of peak to remoulded field vane shear strength) ranged from 3 to 7 with an average of 4.

Multistage K_0 consolidated undrained triaxial compression tests performed on two intact samples of the soft soil collected from the nearby area at a depth of 6.4 m indicated an effective angle of friction $\varphi'_{tr} = 34°$ and an effective cohesion $c' = 8$ kPa.

Two incremental loaded oedometer tests were performed on specimens from 2.6 and 4.5 m depths. The tests showed the compressibility of the soft soil layer in terms of the modulus number, $m = \frac{\Delta\sigma'_v}{\Delta\varepsilon_v}$, to be about 8, corresponding to a compression ratio, CR $= \frac{\Delta\varepsilon_v}{\Delta\log\sigma'_v}$, of 0.29. The recompression modulus number, m_r, was about 55, corresponding to a recompression ratio (RR) of 0.04. The coefficient of consolidation, c_v, was about 0.7 m^2/year, the coefficient of permeability k was about $4 \cdot 10^{-10}$ m/s, and the pre-consolidation stress σ'_{pc} was on average about 20 kPa above the in situ vertical effective stress, which corresponds to an overconsolidation ratio (OCR) at 2.6 and 4.5 m depths of about 2.1 and 1.7, respectively. The apparent pre-consolidation of the soft gyttja is likely to be primarily a result of long-term creep-induced strains. In this connection, the creep index $C_{\alpha\varepsilon}$ was found to increase from approximately 0.006 at the in situ vertical effective stress level

Fig. 2. Representative oedometer compression curve based on end of consolidation vertical strain ε_{100} values and variation in the creep index $C_{\alpha\varepsilon}$ with stress level (specimen depth of 2.6 m, in situ vertical stress $\sigma'_v \sim 18$ kPa, initial water content, $w_0 = 108\%$, and liquid limit, $w_L = 107\%$). RR, recompression ratio; CR, compression ratio.

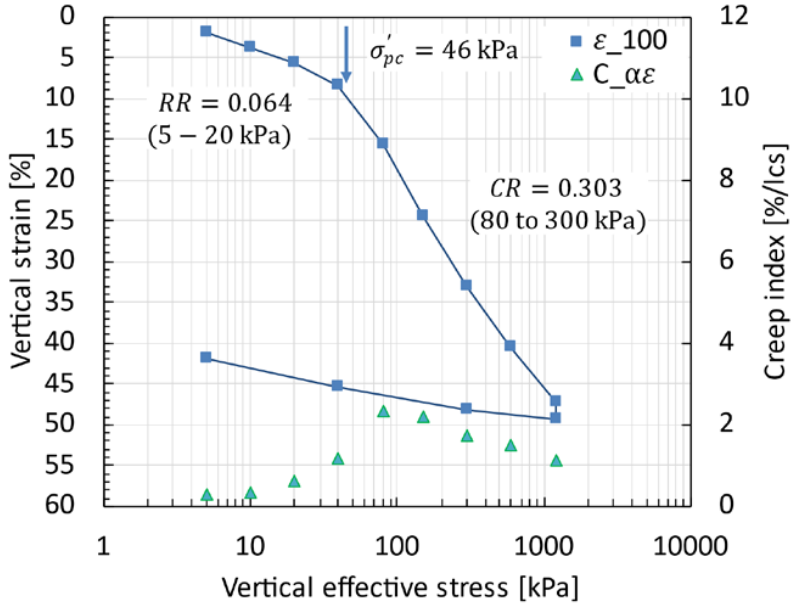

to a maximum value of approximately 0.024 for a stress level around the pre-consolidation stress. Figure 2 shows the compression curve and variation in creep index for the specimen taken at a depth of 2.6 m.

Figure 3 shows results of two CPTU soundings pushed 2 weeks prior to pile installation and located 1 m from the uncoated steel pile and the bitumen-coated precast concrete pile, respectively. The local distinct peaks in cone resistance may be attributed to presence of shell fragments. A cone factor, N_k, of 9 correlated the cone stress, q_t, to vane shear strength. The pore pressure measurements showed the pore pressures in the sand to be hydrostatically distributed with a 0.6 m artesian head.

2.2. Test setup and instrumentation

The test piles (installed on 3 July 2018) consisted of two 406 mm diameter (8 mm wall thickness) steel piles (STP1 and STP2) and two 400 mm square precast concrete piles (CTP1 and CTP2). All piles were driven with a 70 kN Junttan hammer through the soft soil to about 3 m into the sand. Piles STP1 and STP2 were driven to 13.8 m depth and piles CTP1 and CTP2 to 12.8 m depth. The penetration through the soft soil was by the weight of the hammer and pile alone. Piles STP1 and CTP1 were without bitumen coating, while the upper lengths of piles STP2 and CTP2 were coated with a 1 mm thick layer of 80/100 Penetration Grade bitumen between the ground surface and the depths of 10.8 and 9.8 m, respectively. Figure 4 shows a photo of the test piles taken just after installation.

Figure 5 shows the test piles and the ground monitoring system comprising several VW piezometers and settlement stations. The embankment footprint base and upper surface areas were 10 m × 19 m and 6 m × 15 m, respectively. Note the increase in thickness of the soft soil layer from approximately 8 m at CTP2 to approximately 10 m at STP1. It should also be noted that vertical drains were present in the ground approximately 10 m from the long edge of the embankment. These were previously installed as part of a planned ground improvement scheme of the surrounding harbour area.

The pore water pressures were measured using low air-entry VW piezometers installed at 2.6, 5.8, 9.0, and 12.1 m depth on a single string at the centre of the test area using the fully grouted installation method. The grout consisted of water, cement, and bentonite in 8:1:1 ratios by weight. Laboratory tests on similar grout mixture showed an undrained shear strength of approximately $c_{u,UU} = 9$ kPa from unconsolidated undrained (UU) triaxial tests, while the coefficient of permeability was determined to be $k = 3 \times 10^{-8}$ m/s from constant head flow tests, both obtained after 31 days of curing. Two stand-pipes were also installed with intake zones at 6.3 and 10.0 m depth. The water levels were monitored using Diver water level loggers.

The settlements at different depths were monitored by magnetic extensometers (six-leaf spider magnets) installed at 1.2, 3.6, 6.0, 8.4, 9.7, and 14.6 m (datum magnet) depth in-between test piles CTP1 and CTP2, roughly 3 m from the centre of the loaded area. Additionally, two settlement plates were installed at about 0.4 m depth at either end of the lengthwise cross-section of the test area to observe possible differences in the near-surface settlements resulting from the variations in the thickness of the soft soil layer. The datum magnet (1.8 m below CPT1 toe) served as "zero" reference to all settlement gauges. The pile installation of all four piles took about 8 h.

2.2.1. Steel's test pile

The instrumentation of the steel piles and the precast concrete piles is shown in Figs. 6A and 6B, respectively. In

Fig. 3. CPTU diagrams.

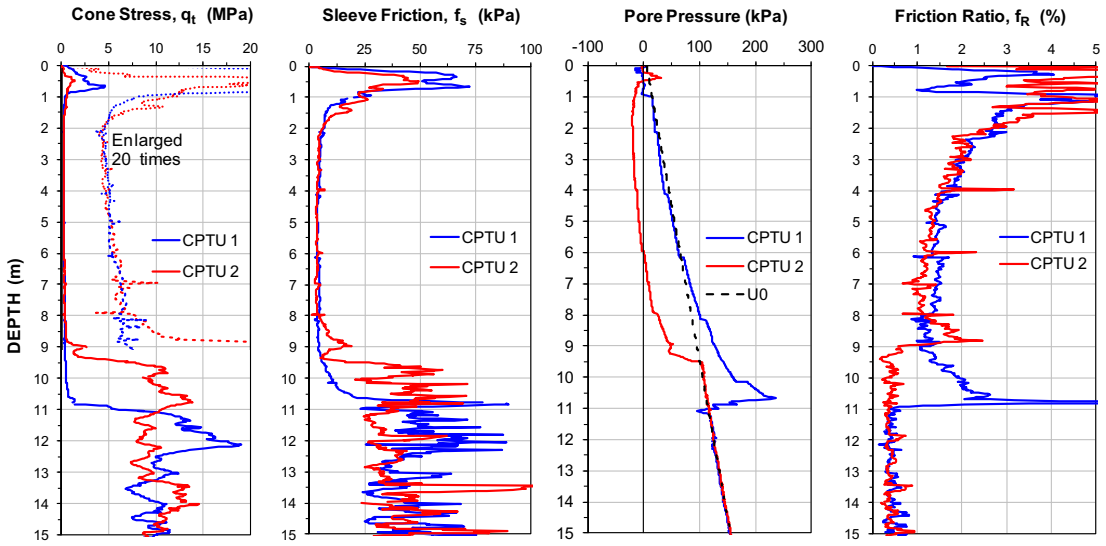

Fig. 4. Photo of test piles after completed installation.

the steel piles, one pair of diametrically opposite surface-mounted VW strain gauges was placed at four depths: 1.0, 5.9, 10.8, and 13.3 m, respectively, and fitted with thermistors for monitoring of gauge temperature. Additionally, the steel test piles were instrumented with two pairs of opposite mounted strain DFOS cables and one pair of opposite mounted temperature DFOS cables. A BRUsens V9 cable was used as strain DFOS cable and a BRUsens Temperature 85 °C cable was used as temperature DFOS cable. Six Ø 10 mm steel rebars were welded (one side intermittent fillet weld with the weld length of 50 mm and the pitch of 100 mm) along the test piles as a guide and protection for all the DFOS cables. The strain DFOS cables were pre-strained to about 1100 $\mu\varepsilon$ prior to being glued in place using Araldite 2012 epoxy. The VW strain gauges were protected by an angle iron welded to the steel piles. Both steel test piles were supplied with a flat pile shoe.

2.2.2. Precast concrete test piles

The concrete piles were cast 14 months before driving. The piles were instrumented with pairs of diametrically oppo-site surface-mounted VW strain gauges at four depths: 1.2, 5.5, 9.7, and 12.3 m, respectively. Resin anchor end blocks were installed in pre-cut spots on the surface and the VW strain gauges and cables were protected by filling the cuts with a high-strength repair mortar. Unfortunately, the VW strain gauges in the concrete piles malfunctioned. The piles were also equipped with two pairs of diametrically opposite surface-mounted strain DFOS cables and one temperature

Fig. 5. Test area with monitoring instrumentation, test piles, and fill embankment.

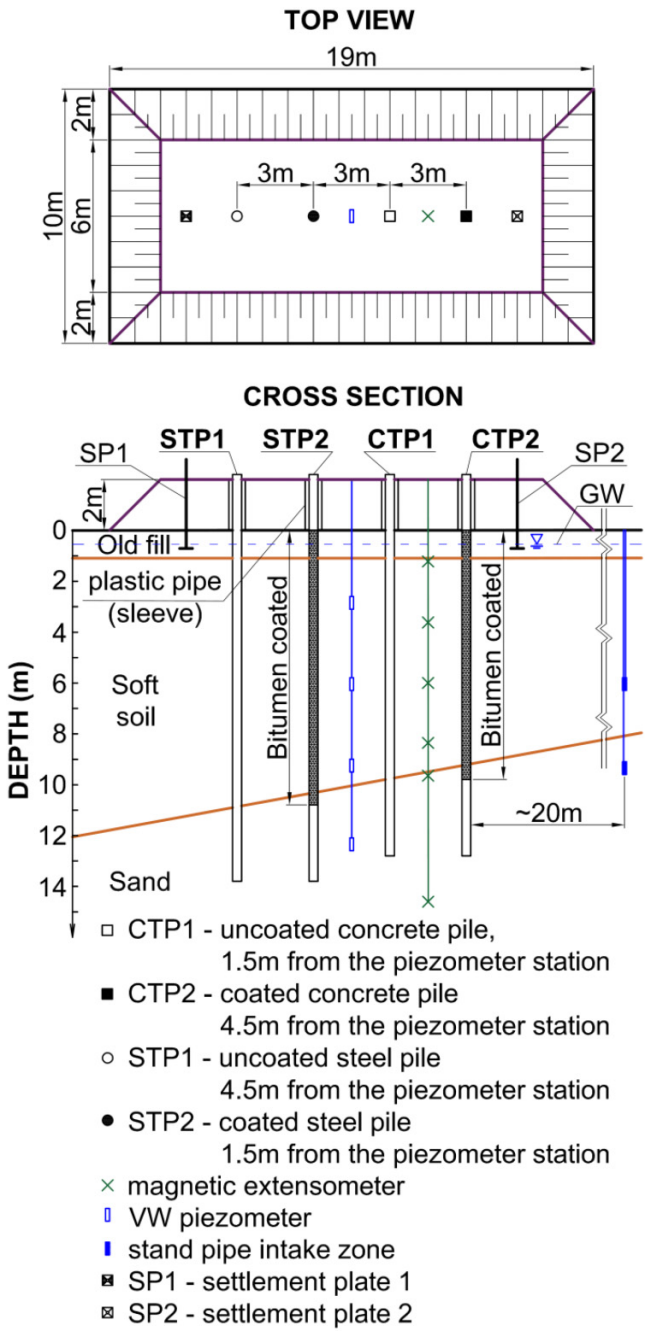

DFOS cable. A BRUsens V9 cable and a BRUsens Temperature 85 °C cable were used to measure strain and temperature, respectively. The strain DFOS cables were pre-strained to about 1100 $\mu\varepsilon$. The DFOS cables were placed along pre-prepared grooves on the side surfaces of the precast concrete piles and covered with Araldite 2012 epoxy.

2.3. Test programme

The test programme consisted of two phases. Phase 1 addressed the effects due to pile installation, while Phase 2 addressed the effects due to placing the fill embankment (c.f. Fig. 5) around the test piles. In the following section, reference will be made to the start of pile installation (Day 0).

Installation of the ground monitoring systems was completed 12 days prior to pile driving (except two settlement plates that were installed after pile driving). The uncoated steel test pile (STP1) was installed first followed by the bitumen-coated steel test pile (STP2), the uncoated precast concrete pile (CTP1), and the bitumen-coated precast concrete pile (CTP2). The piles were installed with the head 2.2 m above the ground surface.

Installation of the four test piles was completed in less than 1 day, and the effect of pile installation was observed until Day 72 at which point a 2 m high embankment was placed over a 10 m × 19 m footprint area around the test piles with an edge slope of 1:1. Before placing the fill embankment, all four test piles were sleeved with a plastic pipe (Ø 600 mm, 2 m length) to protect them from the fill (c.f. Fig. 5). The fill was completed in two 1 m stages over 2 days. Monitoring continued until 277 days after fill placement (Day 350).

2.4. Obtaining strain in DFOS cables

To obtain mechanically induced strain from DFOS cables, it is necessary to thermally correct the DFOS measurements (Kechavarzi et al. 2016). Unfortunately, due to malfunctioning of the temperature DFOS cables, the temperature correction had to rely on an interpolation of the discrete temperature readings from the VW thermistors. The corrected mechanical induced strain is obtained from eq. 1:

$$\varepsilon_{\mathrm{m}}^{z} = \varepsilon_{\mathrm{t}}^{z} - \left(0.95 \cdot \frac{\Delta T^{z}}{k_{\mathrm{T}}} \cdot k_{\varepsilon} + \Delta T^{z} \cdot \alpha_{\mathrm{L}}\right) \quad (1)$$

where $\varepsilon_{\mathrm{m}}^{z}$ is the mechanical strain at depth z;

$\varepsilon_{\mathrm{t}}^{z}$ is the total (measured) strain at depth z;

ΔT^{z} is the change in temperature at depth z (°C) based on interpolation of readings from VW thermistors;

k_{T} is the temperature conversion factor from temperature to frequency (in this study equal to −0.638 °C/GHz);

k_{ε} is the strain conversion factor from frequency to strain (in this study equal to −6.67 $\mu\varepsilon$/GHz); and

α_{L} is the thermal expansion coefficient of the pile material set as 12.2 and 10.4 $\mu\varepsilon$/°C for the steel and concrete piles, respectively.

The cross-section area was calculated as 0.01 and 0.16 m^2 for the steel and precast concrete test piles, respectively. The elastic modulus, E, was assumed to be 210 GPa for the steel piles, while the elastic modulus of concrete, E_{c}, for the precast concrete piles was assumed to be 37 GPa based on the type of concrete (C50/60) and laboratory tension tests conducted on different piles from the same factory (Sørensen 2015) and reinforcement amount.

Further details of the experimental programme including ground conditions, test setup, instrumentation, test program, and data analysis are presented by Kania (2020).

Fig. 6. Cross-section of (A) the instrumented steel test piles and (B) the instrumented concrete piles. DFOS, distributed fibre optic sensors; VW, vibrating wire.

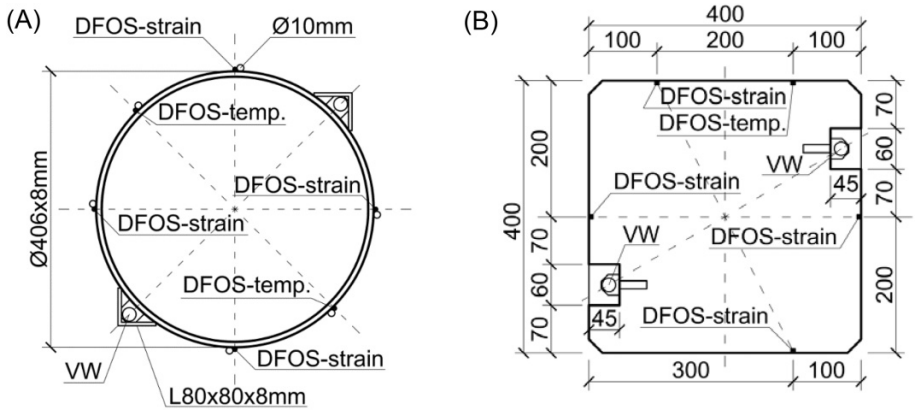

3. Results and discussion

3.1. Instrumentation challenges

The temperature before driving was about 40 °C in the test piles (as warmed by the sun) and reduced after driving to about 10 °C, corresponding approximately to the temperature in the surrounding soil. Unfortunately, due to malfunctioning of the temperature DFOS cables and the non-uniform temperature along the test piles before and immediately after driving, temperature correction of the DFOS strain data during pile installation was not possible. The malfunction-ing of the temperature DFOS cables was likely caused by mechanical strain (Kania et al. 2020) during driving, and further protective measures need to be considered for future use.

The VW strain gauges installed on the precast concrete test piles (CTP1 and CPT2) malfunctioned already before the driving, as a likely result of local cracking, and all VW strain records in the concrete piles were discarded. Ideally, strain gauges should be attached to a sisterbar and embedded in the concrete; however, in this study precast 14-month-old piles were used with the aim to limit the influence of subsequent concrete curing. The use of surface-mounted VW strain gauges proved to be not successful. Only the DFOS gauges provided reliable strain records and only for Phase 2 after fill placement.

For the steel piles (STP1 and STP2), only the VW strain records were reliable for Phase 1. For Phase 2, both the VW strain gauges and DFOS systems provided reliable records.

3.2. Phase 1—influence of pile installation

The first part of the results focuses on the observed influ-ence of pile installation on the ground and the test piles.

For Phase 1, the reference (initial or "zero") readings were taken from all the ground and pile instrumentation before driving the piles.

3.2.1. Pore water pressure changes due to pile installation

Figure 7 shows the excess pore water pressures measured at different depths by the VW piezometer string installed at the centre of the test area. The pore pressures were corrected for measured atmospheric variations (amounting to about 1 kPa on average) and variation in the free water table in the sand layer (about 2 kPa on average). However, they have not been adjusted for heave or settlement of the respective piezometer gauge. The excess pore pressures were referenced to the average pore pressures measured over 4 days before the start of the pile installation. The zero reading of time was taken at 07:45 h shortly before the first pile was installed.

Only small excess pore pressures resulted from soil displacement during installation of pile STP1 4.5 m away from the piezometer string. In contrast, the installation of piles STP2 and CPT1, both 1.5 m away from the piezometer string, resulted in the maximum observed increase of pore water pressures: the piezometers located at 2.6, 5.8, and 9.0 m depth indicated a maximum pore water pressure increase of 19.0, 32.3, and 42.2 kPa, respectively. The measured pore water pressure exceeded locally the total vertical stress from 31% to 44% with an average of 37%. The measured pore pressure dissipated rapidly to an excess pore pressure of about 5 kPa at 5.8 and 9.0 m depth and about 1.5 kPa at 2.6 m depth 65 days after pile driving at which point the pore water pressures are seen to stabilise. The apparent small offsets in the excess pore water pressures after Day 65 may be a result of disturbance during pile driving rather than a lack of equalisation of excess pore water pressures, and this should not have any significant impact on the interpretation of the results. The piezometer installed in the sand at 12.8 m depth registered a temporary increase of pore pressure due to the pile driving. However, the increase of pore water pressure in the sand dissipated within hours after the pile driving.

Figure 8 shows the long-term steady state "hydrostatic" pore pressure profile and measured pore water pressure profiles with depth at selected days after pile driving and subsequent fill placement. The hydrostatic profile was defined according to the readings obtained from the standpipe in the sand layer (artesian pressure) and a water table 0.4 m below ground surface observed in a trench in the old fill layer on Day 0. During the 350 day monitoring period, the water table level in the soft soil layer at a depth of 6.3 m varies from 0.1 to

Fig. 7. Excess pore water pressure due to pile installation and its dissipation with time until Day 65 (Phase 1) prior to placing the fill.

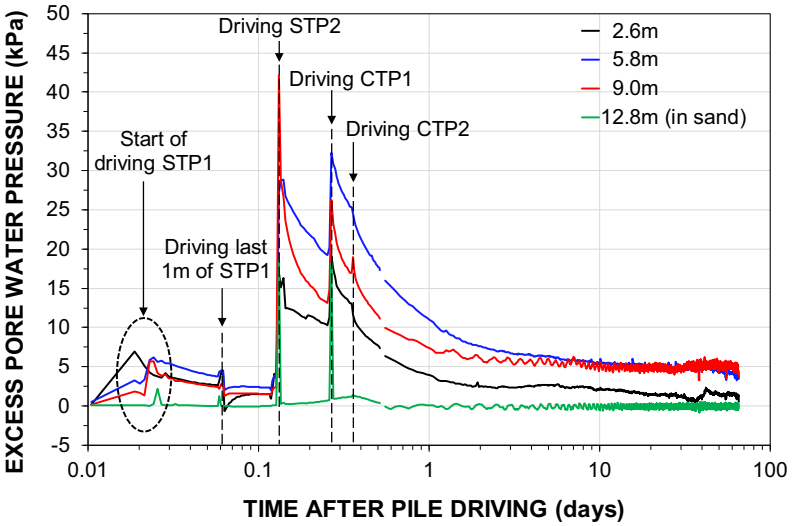

Fig. 8. Pore water pressure (pwp) profiles with depth: hydrostatic, before driving, maximum measured after driving (Phase 1—Day 0), maximum measured after fill placement (Phase 2—Day 73), and final long term (Phase 2—Day 350).

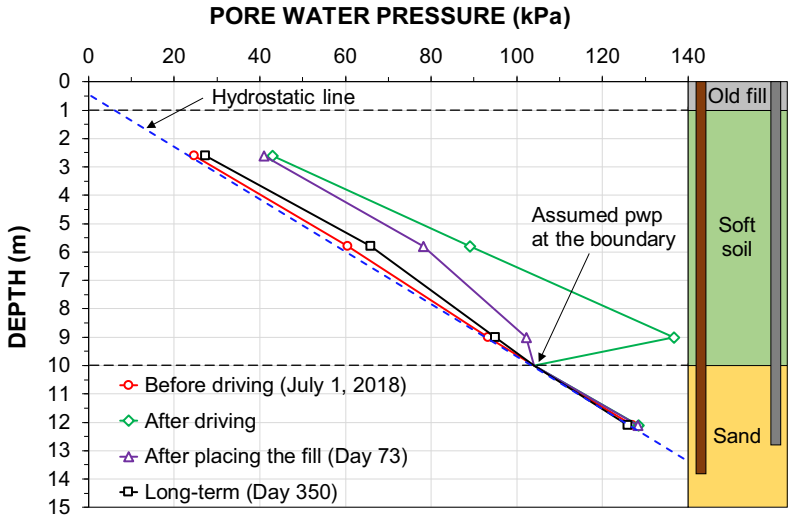

0.7 m with an average of 0.4 m above the ground surface. The hydrostatic head above ground level in the sand layer ranged from 0.3 to 1.2 m with an average of 0.7 m. The pore water pressure profile before driving was generally close to the indicated linear pore water pressure profile, while the greatest offset from the hydrostatic pore water pressure profile was obtained immediately after driving the piles.

3.2.2. Ground movements due to pile installation

Figure 9 presents soil settlements immediately after driving the piles and at Days 9 and 65. The maximum settlement, 17 mm, was obtained from the settlement gauge located at 9.7 m depth. The measurements above 7 m depth indicated that the soil heaved due to the pile installation and then settled back a small amount (about 8 mm) during the 65 day observation period. The maximum heave was 22 mm, as measured at the depth of the first settlement gauge located at 1.2 m depth. The heave decreased with depth. Below 7 m depth, the soil was pushed downward by the pile installation. The maximum downward movement was 18 mm and occurred between 8 and 9 m depth. The downward movement did not change significantly during the Phase 1 observation period (0 through Day 65). The pile head settlements were small (0–1 mm) during Phase 1.

3.2.3. Distribution of axial force and unit shaft resistance after pile driving

Figures 10A–10D show the drag-force distribution obtained from the VW strain gauges along the uncoated steel test pile (STP1) and the coated steel pile (SPT2) immediately and at

Fig. 9. Soil movement profiles immediately after and at selected days after pile installation (Phase 1).

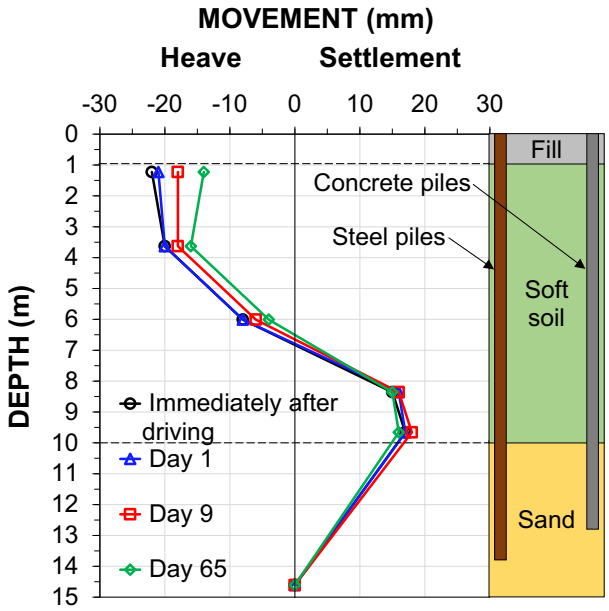

selected days after driving. The reference reading was taken before the pile driving (the pile lying on the ground surface), and all later records of force indicate the change with respect to this reference reading. Positive values denote compression.

Immediately after driving, the largest axial forces in test pile STP1 were 47 and 44 kN (at uppermost and lowermost gauges, respectively). The minimum value of 14 kN was at 5.9 m depth. The force distribution immediately after driving could be explained by rapid compression of the old fill layer and heave of the upper soft soil layer (above 7 m depth). The force increased with time in the middle and at the bottom of the pile. The unit shaft resistance can be calculated as the difference in force between the VW strain gauges acting over the pile shaft area between the gauges. Figure 10C shows the so-calculated unit shaft resistance along the uncoated steel pile (SPT1) immediately and at selected days after driving. The unit shaft resistance of the fill layer and of the soft soil layer are similar to the undrained shear strengths obtained from the field vane test.

As for STP1, the reference reading was taken before driving the pile. As can be seen from the data, the force distribution changed with time. The compressive axial force at the lowermost gauge (13.3 m depth) increased by 30 kN on Day 1 and remained approximately constant until Day 65. This can be explained by the influence of driving of the CTP1 located 3 m from STP2. The strain gauge located within the gyttja (5.9 m depth) recorded a decrease in compression (10 kN to 15 kN) during Phase 1, while the uppermost VW strain gauge (at 1.0 m depth) generally recorded an increase in compression. It is surprising to notice that the VW strain gauges located at 10.8 m depth indicated tension in STP2. Two opposite mounted VW strain gauges located at this depth recorded compression and tension at opposite sides with similar magnitude. This result suggests that lateral deformation of the pile at this depth could have developed. The unit shaft resistance along test pile STP2 immediately and at selected days after driving is presented in Fig. 10D. As expected, the unit shaft resistance within the soft soil layer at Day 65 is low and about 5 kPa. Due to the aforementioned issues with the VW strain gauges located at 10.8 m depth, the calculated unit shaft resistance of the lower part of the pile needs to be interpreted with caution.

3.3. Phase 2—influence of fill placement around the test piles

In the following section, the observed influence of fill placement (Phase 2) on the ground and the test piles is presented.

For Phase 2, all internal strain readings from VW strain gauges and DFOS have been re-zeroed with reference to Day 65 just prior to placing the fill to focus on the changes in axial forces and unit shaft resistance occurring due to fill placement. Similarly, the Phase 2 settlements refer only to the changes due to fill placement.

3.3.1. Pore water pressure changes due to fill placement

Dissipation of excess pore water pressures within the soft soil layer with time after placing the 2.0 m of fill is shown in Fig. 11, becoming stable about 80 days after placing the fill (Day 152 after pile installation). Based on the coefficient of consolidation, c_v, determined from the laboratory oedometer tests, the time to achieve 90% consolidation will be more than 27 years. A possible explanation for the observed fast dissipation of excess pore water pressures and observed similarities in the dissipation at different depths may be due to the aforementioned presence of vertical drains installed about 10 m from the test site in combination with higher hor-izontal than vertical conductivity of the soft soil layer result-ing from possible presence of interbedded layers with high content of shell fragments. The piezometer located at 5.8 m depth recorded some unexpected increase of pore water pres-sure between Days 157–161 and Days 171–232. The cause is not known, but it was probably unrelated to the test piles and fill; hence, the data have been removed in Fig. 11. The pore pressure profiles after fill placement and long-term (Day 350) are shown in Fig. 8 together with the pore pressure profiles after pile driving.

3.3.2. Ground settlements due to fill placement

Figure 12 presents the measured distribution of soil settlements at selected days due to the placing of the fill and the primary consolidation soil settlement $\delta_{c,ult}$ calculated at the centre of the test site based on the average RR and CR given previously. Settlement of the overconsolidated soft soil layers was calculated according to eq. 2:

$$(2)\qquad \delta_{c,ult} = \sum \left[RR \cdot H \cdot \log\frac{\sigma'_{pc}}{\sigma'_{z0}} + CR \cdot H \cdot \log\frac{\sigma'_{z0} + \Delta\sigma'_z}{\sigma'_{pc}} \right]$$

Fig. 10. Distribution of axial force and unit shaft resistance from vibrating wire strain gauges immediately and at selected days after driving (Phase 1) along the (A) uncoated (STP1) (Figs. 10A and 10C) and (B) coated (STP2) steel piles (Figs. 10B and 10D).

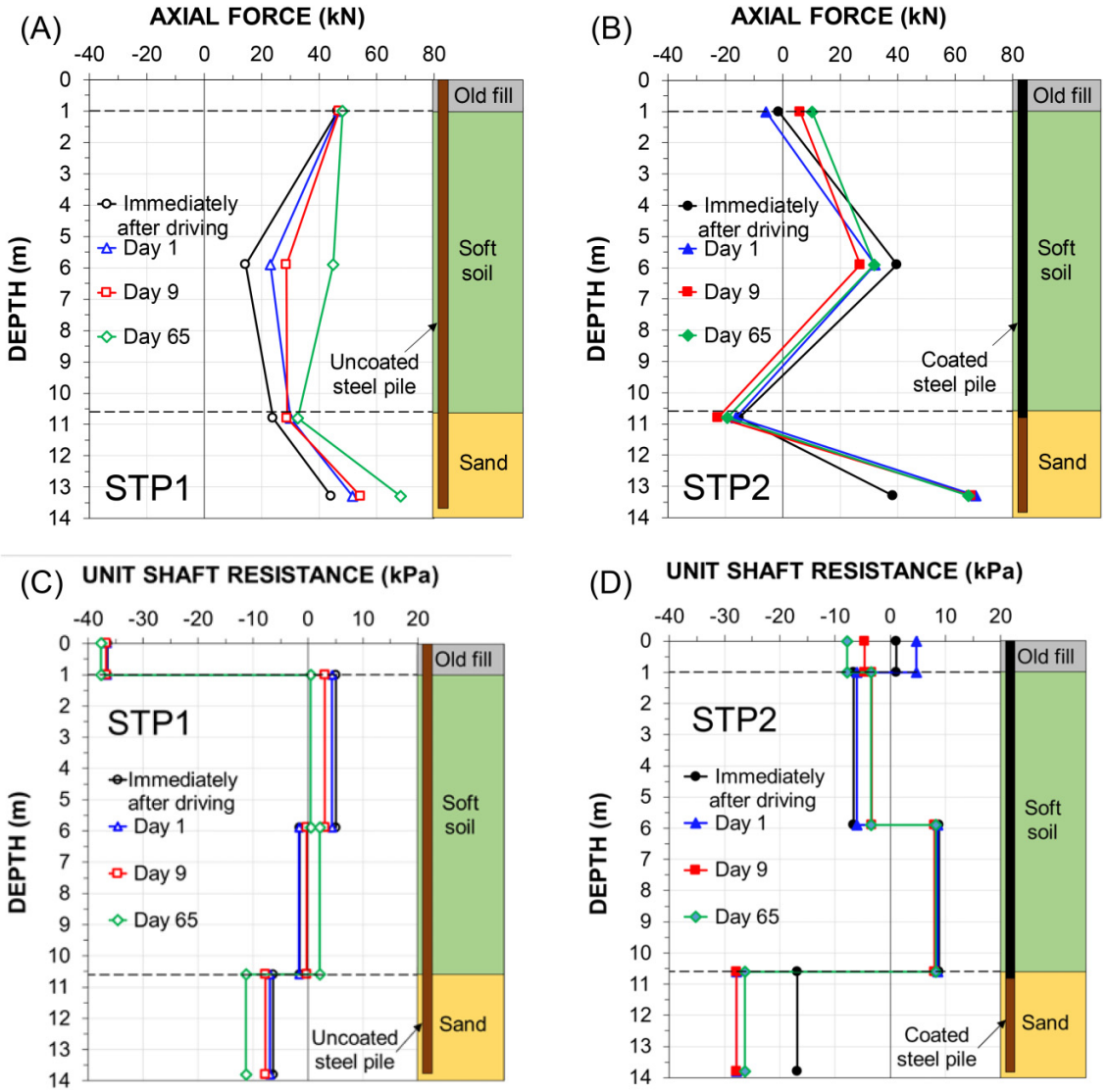

where for each sublayer, H is the thickness of the sublayer, σ'_{z0} is the in situ vertical effective stress, σ'_{pc} is the preconsolidation pressure, and $\Delta\sigma'_z$ is the change in vertical effective stress due to fill placement at the depth z of the sublayer. Note that σ'_{pc} in eq. 1 was replaced with $\sigma'_{z0} + \Delta\sigma'_z$ for layers with $\sigma'_{z0} + \Delta\sigma'_z < \sigma'_{pc}$.

The stress distribution $\Delta\sigma'_z$ due to the fill placement (embankment) was calculated using the equation given by Osterberg (1957) based on integrating the Boussinesq solution and later verified by calculations employing UniSettle4 software (Goudreault and Fellenius 2011). The calculation gave a predicted stress change of 36 kPa at the top of the soft soil reducing nonlinearly to approximately 16.5 kPa at the base.

As expected, the settlement due to the consolidation process occurred mainly in the soft soil layer.

The observed settlements due to the fill placement are shown in Fig. 13. It can be seen that the soft soil was still settling on Day 350, 277 days after placing the fill albeit at decreasing rate. The placing of the fill caused only small settlement (3 mm) in the sand (gauge located at 9.7 m depth), while the settlement gauges located at 1.2, 3.6, 6.0, and 8.4 m depth recorded 173, 81, 39, and 11 mm settlement, respectively, at Day 350. The recorded movements of the ground surface near the settlement plates indicated little difference in the settlements across the test site area, despite the different thickness of the soft soil layer.

Only small settlement of the pile heads (1–3 mm) occurred during Phase 2, representing the pile compression. Hence, the recorded ground settlement can be taken to represent the relative movements between the piles and the surrounding soil.

The large and continued settlements observed in the soft soil layer with time after the apparent dissipation of excess pore water pressures indicate the presence of significant secondary compression. This on the other hand indicates that

Fig. 11. Excess pore water pressure (e.pwp) dissipation with time in Phase 2 after fill placement.

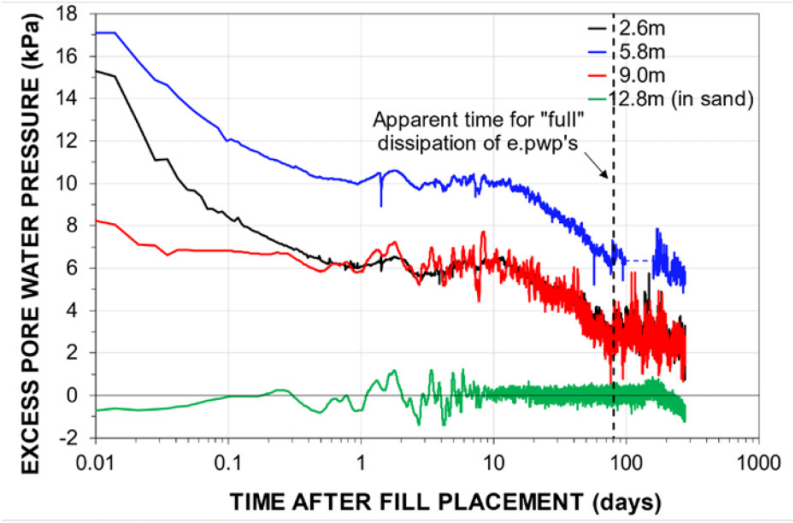

Fig. 12. Measured soil movement profiles due to placing of the fill (Phase 2–Day 73 after pile driving) at selected days after driving compared with the calculated primary consolidation settlement.

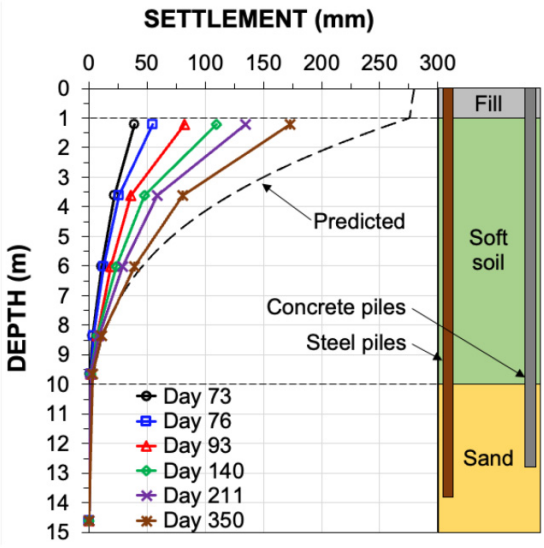

Fig. 13. The settlement of individual gauges with time after pile driving and subsequent fill placement on Day 73 (Phase 1 and Phase 2).

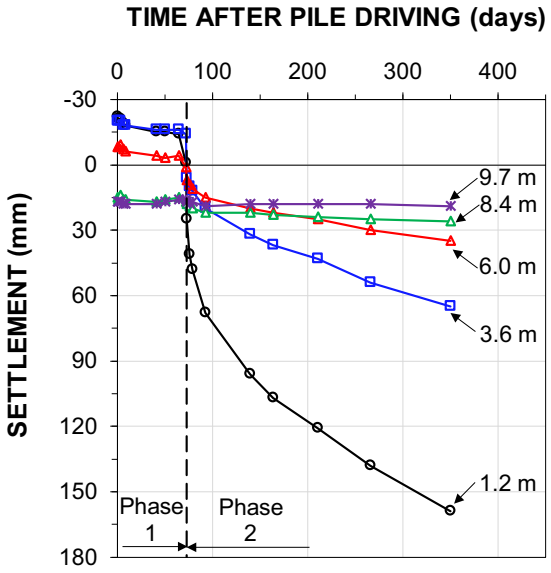

the primary consolidation settlements were governed by a larger reloading stiffness and smaller changes in effective stresses from the fill placement than that assumed in the theoretical calculations. The observed total settlement of the soft soil layer was approximately 57 mm after the indicated full dissipation of excess pore water pressures on Day 152 (80 days after fill placement) until Day 350 (277 days after fill placement). Over the same period, the calculated creep settlements are of similar magnitude as they range between 30 and 117 mm based on the increase in creep index from a minimum value at the in situ stress to a maximum value at the pre-consolidation stress.

3.3.3. Axial force distribution resulting from fill placement

Figure 14A presents the force distribution along the uncoated (STP1) and bitumen-coated (STP2) steel test piles immediately (Day 73) and 277 days after placing the fill (Day 350) as obtained from DFOS strain sensors. As shown in Fig. 14A, the force distributions immediately after placing the fill were the same along the uncoated and bitumen-coated piles. With time, the force increased in the uncoated piles and decreased in the bitumen-coated pile. The obtained long-term maxi-mum drag force on the uncoated and bitumen-coated piles were 87 and 24 kN, respectively. Hence, the bitumen coating

Fig. 14. Force distribution from distributed fibre optic sensor data in Phase 2 along (A) the uncoated (STP1) and bitumen-coated (STP2) steel pile immediately (Day 73) and 277 days after placing the fill (Day 350) and (B) the uncoated precast concrete pile (CTP1) at selected days after placing the fill.

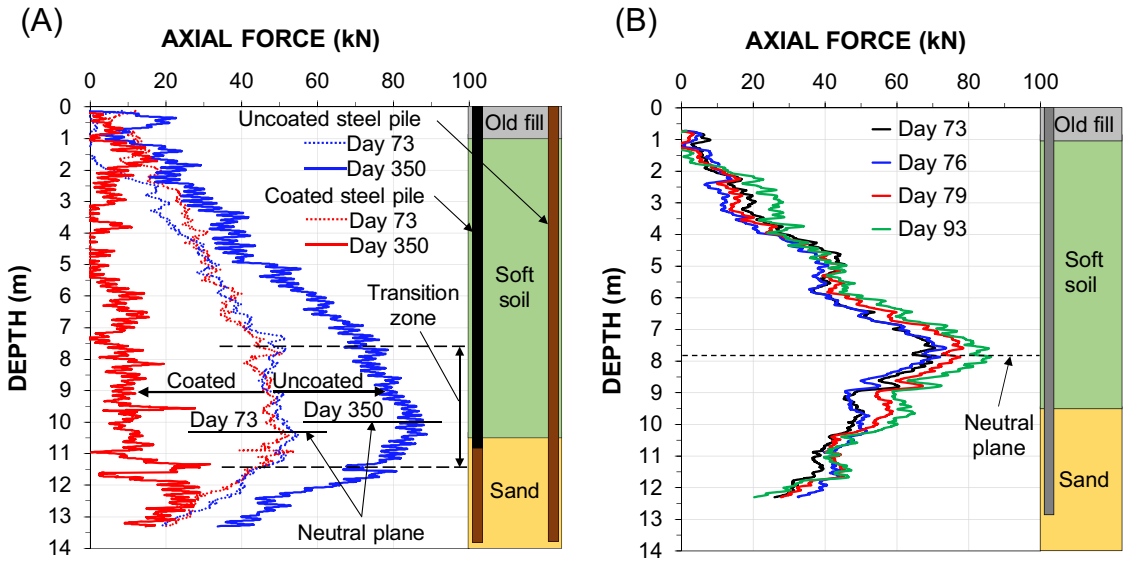

resulted in an approximate 73% reduction in the maximum drag force. This result was confirmed by the VW strain gauges mounted on the uncoated and bitumen-coated steel piles.

The N.P. along the uncoated steel pile was located in the soft soil layer and moved up slightly with time (by about 0.3 m between Day 73 and Day 350). This finding is in agreement with Endo et al. (1969) who also observed that the N.P. moved up with time. The transition zone (277 days after placing the fill) on the uncoated steel pile extended from about 2.3 m above the N.P. (7.8 m depth) to about 1.4 m below the N.P. (11.5 m depth), corresponding to about 3.7 m total length. Disregarding the occurrence of the transition zone would result in an overestimation of the maximum drag force. In contrast, it is difficult to determine the transition zone (277 days after placing the fill) along the bitumen-coated pile.

Figure 15 shows the development of axial force at 5.9 m depth (average value) obtained from two opposite mounted VW strain gauges along the uncoated steel pile (STP1) and bitumen-coated steel pile (STP2). The force magnitudes are seen to be similar during the fill placement. During the first 8 days after placing the fill, the force on the uncoated pile was constant (about 30 kN). Afterwards, it increased in parallel with the observed decrease of excess pore water pressure (see Fig. 11). Interestingly, the force on the uncoated pile (STP1) was still increasing even after dissipation of excess pore water pressure. In contrast, the drag force on the bitumen-coated pile (STP2) significantly reduced during the first 8 days after placing the fill (reaching a value of 4 kN) and did not show significant change afterwards. The results clearly highlight the rate dependent viscous nature of bitumen coating; under high ground movement rates (relative to pile movements), as is the case immediately after fill placement, the bitumen acts as a stiff medium with insignificant effect on the mobilised shaft resistance. In contrast, at lower

Fig. 15. Axial force at 5.9 m depth from vibrating (VW) strain gauges along the uncoated (STP1) and bitumen-coated (STP2) steel pile in Phase 2 after start of fill placement (Day 72).

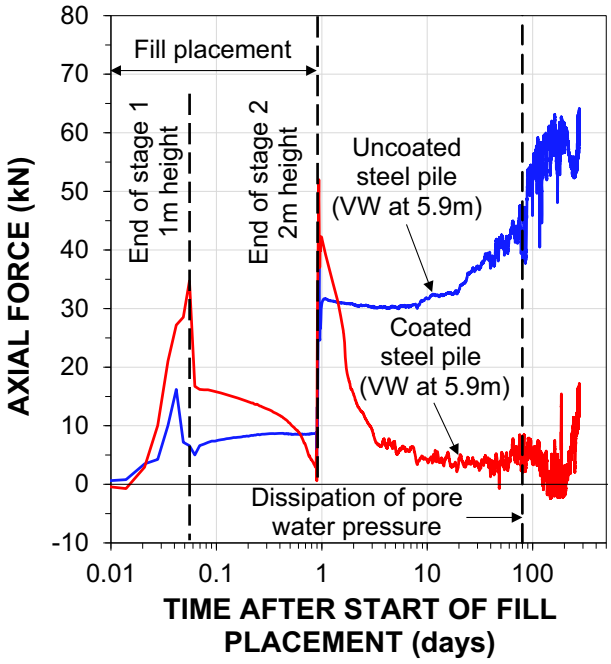

ground movement rates, the viscosity of the bitumen leads to a significant reduction of the shaft resistance and the drag force. These results support other research (Fellenius 1975, 1979; Fukuya et al. 1982).

Figure 14B shows the force distribution along the uncoated precast concrete pile (CTP1) at an early stage of the second phase (up to 20 days after placing the fill). The strain profiles

Fig. 16. Unit shaft resistance distributions from distributed fibre optic sensors strain data with depth in Phase 2 along (A) the uncoated (STP1) and the bitumen-coated (STP2) steel test pile immediately (Day 73) and 277 days after fill placement (Day 350) and (B) the uncoated precast concrete pile (CTP1) immediately (Day 73) and 20 days after fill placement (Day 93).

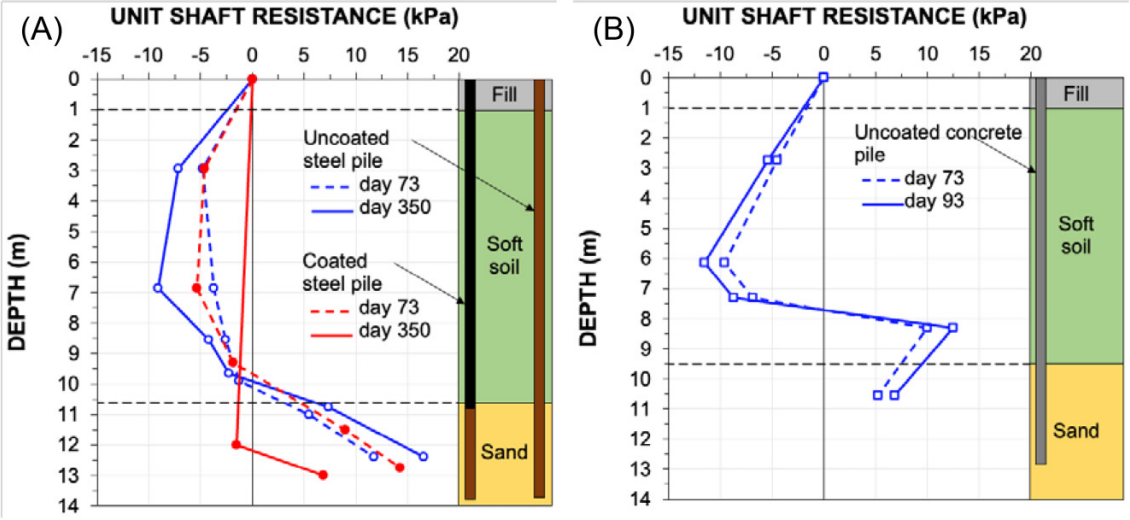

recorded from the DFOS strain sensors after this stage were scattered and their interpretation was difficult. A possible explanation for this could be the existence and evolution of cracks of the precast concrete test piles (Kania et al. 2020). As shown in Fig. 14B, the N.P. was located at about 7.8 m depth and the transition between negative and positive direction of shear was distinct at that stage. The maximum recorded drag force of 86 kN occurred 20 days after placement of the fill (Day 93). The slightly higher location of the N.P. for the uncoated concrete pile compared to uncoated steel pile is not linked to greater settlement of the concrete pile but is likely resulting from different ground movements profiles around the piles caused by variations in ground conditions.

The evolution of cracks and the impact on the DFOS strain sensor readings was even greater along the bitumen-coated precast concrete pile (CTP2). Thus, the interpretation of the strain DFOS data was difficult, and the results from test pile CTP2 are not presented in this paper.

4. Analysis of results, Phase 2—influence of fill placement

In the following section, the results of Phase 2 are analysed in more depth with the aim to quantify and characterise the development of unit shaft resistance along the test piles in subsiding soil and to get a better understanding of the governing mechanisms.

4.1. Unit shaft resistance distribution

Figure 16 shows the unit shaft resistance distributions with depth as obtained from DFOS strain data at selected days after placing the fill (Fig. 16A) along the uncoated (STP1) and bitumen-coated (STP2) steel test pile and (Fig. 16B) along the uncoated precast concrete pile (CTP1). The average unit shaft resistance has been determined for a number of sub-layers from the variation in the axial force distribution from the DFOS strain data. The unit shaft resistance distributions along the uncoated and bitumen-coated steel test pile immediately after placing the fill (Day 73) were similar. With time, the unit shaft resistance (in both negative and positive directions) increased along the uncoated steel test pile. In contrast, the unit shaft resistance along the bitumen-coated steel pile decreased with time. The transition between negative and positive directions of shear was more gradual on the uncoated steel test pile than that for the uncoated precast concrete test pile.

4.2. Development of the unit shaft resistance along the steel test piles

The development of average negative skin friction with time along the uncoated and bitumen-coated steel piles within the soft soil layer is presented in Fig. 17, as de-termined for a number of sublayers from the variation in the axial force distribution from the DFOS strain data. The negative unit shaft resistance on the uncoated and the bitumen-coated pile immediately after placing the fill was about 4–5 kPa. These values corresponded to the remoulded undrained shear strength determined from the field vane shear tests. About 8 days after placing the fill, the negative unit shaft resistance on the uncoated pile started to increase along both determined layers (0–5.9 and 5.9–7.8 m depth) as a result of dissipation of excess pore water pressure and asso-ciated increases in the effective stresses in the soil. The unit shaft resistance was observed to still increase after dissipa-tion of excess pore water pressures, reaching a value of 7–9 kPa (Day 350, 277 days after placing the fill). In contrast, the negative unit shaft resistance on the bitumen-coated pile de-creased during the first 8 days, reaching a stable value around 1 kPa. Gradual (creep) settlement may result in total horizon-tal stress changes around the pile, which could be an expla-nation for the observed long-term increase in the unit shaft

Fig. 17. Back-calculated distribution of (A) unit negative skin friction and (B) beta-coefficient from distributed fibre optic sensors strain data along the uncoated (STP1) (at two determined soil layers above N.P.) and the bitumen-coated (STP2) (entire bitumen coated section of the pile) steel pile in Phase 2 after fill placement (Day 73).

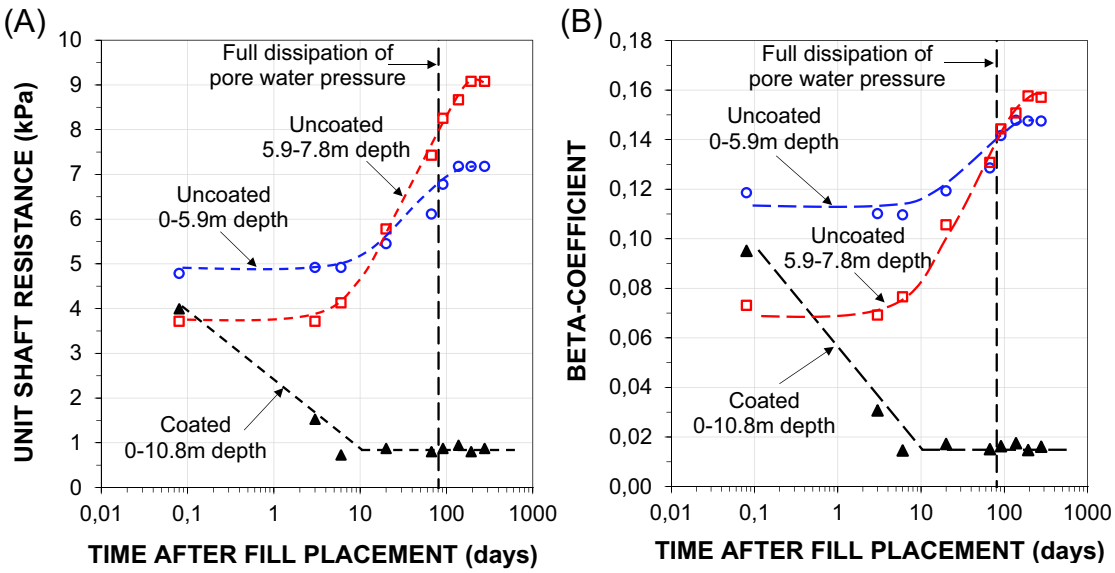

resistance along the uncoated pile after full dissipation of the excess pore water pressure (Fellenius 1979, 2023). The reducing rate of increase in negative unit shaft resistance with time appears to be linked to the gradual reduction in the settlement rate. That is, the shaft shear resistance for an uncoated pile is a function of the shear movement, whereas, for a bitumen-coated pile, it is a function of shear rate.

Figure 18 shows the development of negative unit shaft resistance on the uncoated and bitumen-coated steel pile against the rate of relative movement between the pile and the soil and against absolute movement. For the coated steel pile, the unit shaft resistance reduced with reducing shearing rate until the unit shaft resistance reached 1 kPa as the rate of relative movement reduced to about 2 mm/day. The results suggest that the development of unit shaft resistance for the coated pile was primarily governed by the shearing rate as would be expected due to the viscous nature of the bitumen coating. In contrast, the development of unit shaft resistance for the uncoated pile with time after fill placement was not influenced by the reducing shearing rate.

The effect of bitumen coating is further supported by a series of interface laboratory direct shear tests conducted on undisturbed samples from the test site (Kania et al. 2021). The results highlight a significant reduction in the mobilised shear stress to approximately 1 kPa, independently of normal stress, when the soft soil is sheared against bitumen at very low displacement rates (0.01 mm/h). At increasing displacement rates, the shear stress was found to increase significantly to become dependent on normal stress. At high displacement rate (100 mm/h), the mobilised shear stress was of similar magnitude to that recorded when the soft soil was sheared against concrete at equal normal stress level.

Figure 18B shows the development of negative unit shaft resistance along determined layers on the uncoated and bitumen-coated steel piles versus relative movement between the pile and the surrounding soil. The measured relative movement between pile and soil can be expected to be linked to volumetric compression of the soft soil due to dissipation of excess pore water pressures and additional creep-induced reductions in void ratio. As can be seen, the maximum mobilised unit shaft resistances at different depths along the uncoated and bitumen-coated steel piles occurred at different relative movement. For the uncoated pile, the observed differences may be explained by an increase in soil stiffness and reduced settlement with increasing depth.

4.3. Comparison between the uncoated steel and precast concrete pile

In analysing shaft resistance, it is useful to apply the beta-coefficient, which is the unit shaft resistance normalized to (divided by) the effective vertical stress with respect to fill placement and measured excess pore water pressure. Immediately after placing the fill, the beta-coefficient ranged from 0.07 to 0.12 along the uncoated length and 0.10 on aver-age along the bitumen-coated length for the uncoated and bitumen-coated piles, respectively. With time, 277 days af-ter placing the fill (Day 350) the average beta-coefficient increased to about 0.15 for the uncoated pile, while it decreased to about 0.02 for the bitumen-coated pile.

Figure 19 shows the development of the average beta-coefficient (defined as the unit shaft resistance divided by the vertical in situ stress) and the excess pore water pressure dissipation with time. The increases of the beta-coefficient along the uncoated precast concrete and steel pile are similar. Considering the beta-coefficient along the uncoated precast concrete pile as a reference (material surface factor of 1.0), the material surface factor for steel can be calculated as 0.7. For

Fig. 18. Development of negative skin friction from distributed fibre optic sensors data along the uncoated (STP1) and bitumen-coated (STP2) steel pile against (A) rate of relative movement and (B) relative movement at determined soil layers in Phase 2 after fill placement (Day 73).

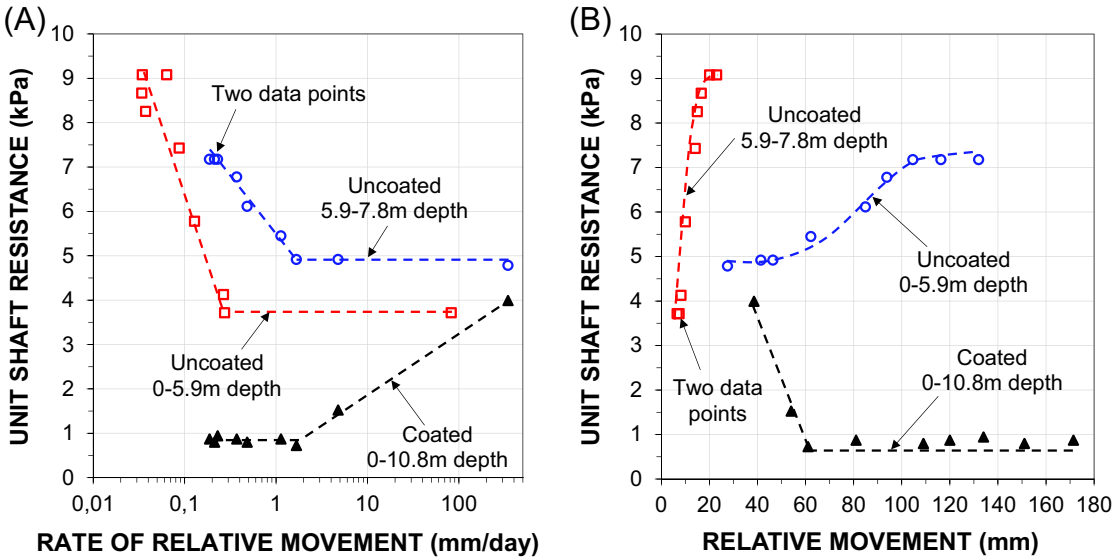

Fig. 19. Comparison of the development of the average beta-coefficient along the uncoated precast concrete pile (CTP1) and the uncoated steel pile (STP1) in Phase 2 after fill placement (Day 73). The secondary scale is showing the average excess pore water pressure dissipation with time.

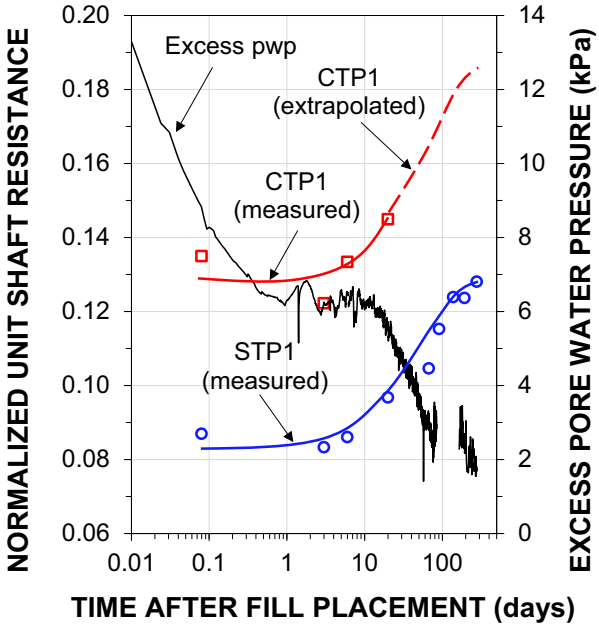

comparison, a factor of 0.8 was determined from the interface direct shear tests reported by Kania et al. (2021). The calculated material surface factors for steel are also consistent with those proposed by Kulhawy (1983). Based on the ratio of 0.7, the long-term increase of the beta-coefficient was extrapolated (dashed line). The maximum obtained beta-coefficient for the uncoated steel (extrapolated) and uncoated precast concrete pile was 0.13 and 0.19, respectively. The difference may be due to the clay being able to drain into the concrete pile and thus gain strength to 40% over that of the shear force along the steel pile.

5. Conclusions

The following conclusions can be drawn from this case study.

(1) Owing to the spatial resolution of the used DFOS, it was possible to accurately determine the location of the N.P. and distinguish the transition zone for the uncoated piles. For the uncoated steel and concrete piles, the N.P. was located just above the boundary between the soft soil and the underlying sand layer, and did not move significantly with time. The transition between negative and positive shaft resistance was observed to be gradual for the uncoated steel pile, while a sharp transition was observed for the uncoated concrete pile.

(2) For the uncoated concrete and steel piles, the development of unit shaft resistance was governed by the relative movement between the pile and soil. The short-term mobilised unit shaft resistance was similar in magnitude to the remoulded undrained shear strength. Furthermore, the results suggest that the observed gradual increase in unit shaft resistance with time was primarily governed by an increase in effective stress resulting from the dissipation of excess pore water pressures in addition to shear strength increase from significant volumetric creep.

(3) The beta-coefficient along the uncoated steel and precast concrete pile was found to be 0.13 and 0.19, respectively. Based on limited measurements prior to full mobilisation of the negative unit shaft resistances, the obtained

material surface factor for steel was determined to be 0.7 (considering the negative unit shaft resistance along the precast concrete pile as a reference with a factor of 1.0).

(4) For the coated pile, the viscous behaviour of the bitumen coating governed the shearing resistance. At large ground movement rates, the bitumen acts as a stiff medium, and the mobilised unit shaft resistance is similar to that seen for uncoated piles. In contrast, at reduced ground movement rates, the slow flow of the bitumen will result in minimal transfer of shear stresses. A 73% reduction in the maximum long-term drag force was observed as a result of the thin (1 mm) bitumen coating applied to the steel pile.

(5) The drag force that developed along the uncoated pile in the about 10 m thick gyttja layer amounted to about 80 kN, a value of no concern for the design of foundations supported on single piles.

Acknowledgements

The authors would like to thank cp test a/s, Per Aarsleff A/S, Centrum Pæle A/S, DMT Gründungstechnik, GmbH, and Innovation Fund Denmark (grant No. 5189-00065B) for providing funding for this study and Per Aarsleff A/S for installing the instrumented test piles and ground monitoring equipment.

Article information

History dates

Received: 14 February 2023
Accepted: 21 November 2023
Accepted manuscript online: 6 December 2023
Version of record online: 21 March 2024

Copyright

Data availability

Data generated or analysed during this study are available from the corresponding author upon reasonable request.

Author information

Author ORCIDs

Kenny K. Sørensen https://orcid.org/0000-0001-9400-7753

Author notes

Jakub G. Kania current affiliation: COWI A/S Denmark.

Author contributions

Data curation: JGK, KKS, BHF
Formal analysis: JGK, KKS, BHF
Funding acquisition: JGK, KKS
Investigation: JGK, KKS
Methodology: JGK, KKS
Project administration: JGK, KKS
Supervision: KKS
Validation: KKS, BHF
Writing – original draft: JGK
Writing – review & editing: JGK, KKS, BHF

Competing interests

The authors declare there are no competing interests.

References

Baligh, M.M., Figi, H., and Vivatrat, V. 1978. Downdrag on bitumen-coated piles. ASCE Journal of the Geotechnical Engineering, **104**(GT11): 1355–1370.

Bjerrum, L. 1972. Embankments on soft ground. *In* Proceedings of the ASCE Specialty Conference on Performance of Earth and Earth-Supported Structures. June 11–14, 1972. Vol. II. Purdue University, Lafayette. pp. 1–54.

Bjerrum, L., Johannessen, I., and Eide, O. 1969. Reduction of negative skin friction on steel piles to rock. *In* Proceedings of the 7th ICSMFE, Mexico, August 25–29. Vol. 2. pp. 27–33.

Endo, M., Minou, A., Kawasaki, I., and Shibata, T. 1969. Negative skin friction acting on steel pipe pile in clay. *In* Proceedings of the 7th International Conference on Soil Mechanics and Foundation Engineering, Mexico, August 25–29. Vol. 2. pp. 85–92.

Fellenius, B.H. 1975. Reduction of negative skin friction with bitumen slip layers. Journal of the Geotechnical Engineering Division, **101**(GT4): 412–414. doi:10.1061/AJGEB6.0005027.

Fellenius, B.H. 1979. Downdrag on bitumen coated piles. American Society of Civil Engineers, ASCE Journal of Geotechnical Engineering, **105**(GT10): 1262–1265.

Fellenius, B.H. 2006. Results from long-term measurement in piles of drag load and downdrag. Canadian Geotechnical Journal, **43**(4): 409–430. doi:10.1139/t06-009.

Fellenius, B.H. 2023. Basics of foundation design—a textbook[online]. Available from www.Fellenius.net [accessed August 2023].

Fellenius, B.H., and Broms, B.B. 1969. Negative skin friction for long piles driven in clay. *In* Proceedings of the 7th International Conference on Soil Mechanics and Foundation Engineering, Mexico, August 25–29. Vol. 2. pp. 93–97.

Fukuya, T., Todoroki, T., and Kasuga, M. 1982. Reduction of negative skin friction with steel tube NF pile. *In* Proceedings of the Seventh Southeast Asian Geotechnical Conference, Hong Kong, November 22–26. pp. 333–347.

Goudreault, P.A., and Fellenius, B.H. 2011. UniSettle Version 4 tutorial with background and analysis examples. UniSoft Geotechnical Solutions Ltd. 85p. Available from. https://www.unisoftgs.com/ [accessed August 2017].

Hutchinson, J.N., and Jensen, E. 1968. Loading tests on piles driven into estuarine clays at the Port of Khorramshahr, Iran, and observations on the effect of bitumen coatings on shaft bearing capacity. Vol. 78. Norwegian Geotechnical Institute Publication. 12p.

Indraratna, B., Balasubramaniam, A., Phamvan, P., and Wong, Y. 1992. Development of negative skin friction on driven piles in soft Bangkok clay. Canadian Geotechnical Journal, **29**(3): 393–404. doi:10.1139/t92-044.

Johannessen, I.J., and Bjerrum, L. 1965. Measurements of the compression of a steel pile to rock due to settlement of the surrounding clay. *In* Proceedings of the 6th International Conference on Soil Mechanics and Foundation Engineering, Montreal, September 8–15. Vol. 6. pp. 261–264.

Kania, J. G. 2020. Soil-pile Interaction in Soft Soils. PhD. Dissertation. Department of Civil and Architechtural Engineering, Aarhus University. ISBN: 978-87-7507-481-5. doi:10.7146/aul.380.

Kania, J.G., Sørensen, K.K., and Fellenius, B.H. 2020. Application of distributed fibre optic cables in piles. Geotechnical Engineering Journal of the SEAGS and AGSSEA, March 2020, **51**(1): 9.

Kania, J.G., Sørensen, K.K., and Fellenius, B.H. 2021. Shear stress between a soft soil and various pile materials. *In* Proceedings of the 74th Canadian Geotechnical Conference. Niagara Falls, September 26–29. 7p.

Kechavarzi, C., Soga, K.B., Battista, N.D., Pelecanos, L., Elshafie, M.Z.E.B., and Mair, R.J. 2016. Distributed fibre optic strain sensing for monitoring civil infrastructure—a practical guide. ICE Publishing, London, UK. 264p.

Klar, A., Bennett, P.J., Soga, K., Mair, R.J., Tester, P., Fernie, R., et al. 2006. Distributed strain measurement for pile foundations. Proceedings of the Institution of Civil Engineers—Geotechnical Engineering, **159**: 135–144. doi:10.1680/geng.2006.159.3.135.

Kulhawy, F.H. 1983. Transmission line structure foundation for uplift-compression loading. Report EL-2870. Electric Power Research Institute.

Okabe, T. 1977. Large negative friction and friction-free piles methods. *In* Proceedings of the 9th International Conference on Soil Mechanics and Foundation Engineering, Tokyo, July 11–15. Vol. 1.pp. 679–682.

Osterberg, J.O. 1957. Influence values for vertical stresses in semi-infinite mass due to embankment loading. *In* Proceedings of 4th International Conference on Soil Mechanics and Foundation Engineering, London, August 12–24. Vol. 1. pp. 393–394.

Savery, A.L. 2019. Gyttja deposits from Randers and Esbjerg—an investigation of composition and geotechnical properties. MSc. report. Department of Geoscience, Aarhus University. 46p.

Sørensen, K.K. 2015. Fuldskala pæleforsøg på Randers havn/full-scale pile testing at Randers Habour, presentation at the Danish Geotechnical Society meeting.